

## Non-reacting Flow Analysis from Combustor Inlet to Outlet using Computational Fluid Dynamics Code

G. Ananda Reddy and V. Ganesan

*Indian Institute of Technology Madras, Chennai-600 036*

### ABSTRACT

This paper describes non-reacting flow analysis of a gas turbine combustion system. The method is based on the solution of Navier-Stokes equations using generalised non-orthogonal coordinate system. The turbulence effects are modelled through the renormalisation group  $k-\epsilon$  model. The method has been applied to a practical gas turbine combustor. The combustion system includes swirler vane passages, fuel nozzles, rotor bleed, customer bleed, air-blast atomiser, swirl cone, and all holes in primary, dilution, dome, flare, and cooling ring. The total geometry has been created using the pre-processors GAMBIT and CATIA, and the meshing has been done using GAMBIT, and the analysis carried out in a FLUENT solver. The interaction between the diffuser and the combustor external flows plays a key role in controlling the pressure loss, air flow distribution around the combustor liner, durability, and stability. The aero gas turbine combustor designs are generally guided by experimental methods and past experience; however, experimental methods are inherently slow, costly, especially at high temperature engine-operating conditions. These drawbacks and the growing need to understand the complex flow-field phenomenon involved, have led to the development of a numerical model for predicting flow in the gas turbine combustor. These models are used to optimise the design of the combustor and its subcomponents, and reduce cost, time, and the number of experiments.

**Keywords:** Non-reacting flow, computational fluid dynamics, combustor, turbulence, continuity, total-pressure loss, static pressure recovery coefficient, swirler, CFD, gas turbine combustion, flow-field phenomenon, diffuser-combustor flow interaction

### NOMENCLATURE

$a$  Sonic velocity

$E$  Energy

$C_{1\epsilon}$  Constants in turbulence dissipation rate equation  
 $C_{2\epsilon}$

$F_i$  Body force

$h$  Enthalpy

$J_p$  Diffusion flux

$k$  Thermal conductivity

$K$  Turbulence kinetic energy

$p$  Static pressure

$t$  Time

$T$  Temperature

$u$	Velocity in X-direction
$v$	Velocity in Y-direction
$w$	Velocity in Z-direction

*Greek symbols*

$\alpha$	Inverse effective Prandtl number
$\delta_{ij}$	Kronecker-delta function
$\varepsilon$	Turbulent dissipation rate
$\mu$	Kinematic viscosity
$\mu_{lam}$	Laminar dynamic viscosity
$\nu_t$	Turbulent viscosity
$\nu_{lam}$	Laminar kinematic viscosity
$\rho$	Density
$\tau$	Shear stress

## 1. INTRODUCTION

The combustor in a gas turbine power plant is one of the main elements, whose operational performance governs the reliability and efficiency of the gas turbine power plant. The aerodynamic process plays a vital role in the design and performance of a gas turbine combustion system. The flow in the combustion chamber is generally complex, due to highly turbulent nature of the flow field, coupled with complex geometric configuration. Further, the additional complications of combustion like fuel evaporation, radiative and convective heat transfer, and chemical kinetics are also involved. The interaction between the diffuser and the combustor external flows plays a key role in controlling the total-pressure loss, flow distribution around the combustor liner, durability, and stability.

The diffuser-combustor flow interaction is governed by several geometric and flow parameters. A dump diffuser system includes the pre-diffuser length and area ratio, the dump gap and expansion ratio, the flow-splits between the dome inner and outer annuli, the velocity distribution, and the turbulence

level at the compressor exit. The flow-split among the outer and the inner annuli, and the central streams are strong functions of the dump gap ratio, which in turn affects the overall combustor total pressure loss. If the dump gap is too small, the flow into the dump region will be accelerated around the cowl-leading edge and the total pressure loss would be higher. If the dump gap ratio is too large, the spillage from the cowl will reduce the pressure recovery in dome region and would cause a higher total pressure loss, because of mixing of the low momentum spillage flow with velocity passage flow in the combustor liner passages. The spillage also causes flow separation from the cowl surfaces, leading to an increase in the total pressure loss.

The subcomponents, such as swirler, atomiser, support struts, locating pins, and fuel nozzle should be designed and placed so that these have minimum effect on the pressure recovery and combustor exit temperature quality. The non-uniformities in the pressure distribution can result in inadequate cooling at various locations, or even cause reversal of the flow direction with consequent overheating of the combustor liner.

As stated, combustor designs are predominantly guided by the experiments and the past experience. Because of the complex geometry flow field and the time-consuming and costly experimental methods, the development of numerical models for predicting flow in a gas turbine combustor has been undertaken. These models are used to optimise the design of the combustor and its subcomponents, and reduce the volume of experimental and tuning work.

The aim of the present research is to:

- Study the flow field in an annular gas turbine combustor for isothermal flow condition.
- To investigate the effect of increasing the inlet velocity on total pressure loss.

## 2. HISTORICAL BACKGROUND

Crocker,<sup>1</sup> *et al.* performed a computational fluid dynamics (CFD) calculation for a model combustor,

from the compressor exit to the turbine inlet. The model includes an air-blast atomiser, dome, and liner walls with dilution holes and cooling louvers. The coupled model describes the flow-splits and the flow conditions for openings into the combustor liner. The analysis illustrates the influence of flow non-uniformities on the static pressure distribution around the liner walls and the resulting effect on flow-splits and liner wall temperatures. The influence of non-luminous radiation and thermal barrier coatings on the liner wall temperatures is also examined.

Sokolov<sup>2</sup>, *et al.* carried out mathematical modelling of annular gas turbine combustor. The model describing the axisymmetric swirling flow with diffusive combustion was based on numerical and experimental investigations of local and general characteristics of the flow in an annular combustor with swirling air jets. It was shown that with an increase in the degree of blockage in the channel, the relative length of the re-circulation zone was increased, and with an increase in the angle of swirl, the relative length of the re-circulation zone was decreased. They observed that increased angle of swirl had a marked effect on the intensity of turbulence, which at  $\pm 60^\circ$  reached almost 100 per cent, while it didn't exceed 30 per cent with a straight stream flow. It was found that the results of calculations and experiments agreed within the limits of measurement error.

Su and Zhou<sup>3</sup> carried out a numerical study on combustor-diffuser flow interaction using the KIVA-3V code. The simulation was based on the solution of Navier-Stokes equations with phenomenological models of turbulence, spray generation, and chemical reactions. The swirler was simplified in terms of the conservation of mass and momentum. The static pressure recovery coefficients along the inner and the outer walls of the pre-diffuser and combustor casing were obtained from the numerical solutions and these agreed well with the published measured data. The flow fields in the axial and the circumferential directions were analysed.

Relation and Battaglioli<sup>4</sup> carried out numerical simulation on non-reacting flows for industrial gas

turbine combustor geometries. They evaluated the application of the CFD to calculate the flow fields in industrial combustors. The standard  $k-\epsilon$  turbulence model and a modified version of the  $k-\epsilon$  turbulence model, in which a second time scale was added to the turbulent dissipation equation, were compared. The results of the CFD calculation thus obtained were compared with the experimental data<sup>5-10</sup>. For the present case study, the standard  $k-\epsilon$  model diffuses the swirl and the axial momentum, which results in the inconsistent prediction of the re-circulation zone for the test cases. However, the modified  $k-\epsilon$  model showed an improved prediction of the location, shape, and size of the centreline re-circulation zone. The large swirl and the axial velocity gradients, which were diffused by the standard  $k-\epsilon$  model, were preserved by the modified model, and a good agreement was reached between the calculated and the measured axial and swirl velocities. The over prediction of the turbulent eddy viscosity in regions of high shear, which is a characteristic of the standard  $k-\epsilon$  model, was found to be controlled by the modified turbulence model.

Ganesan and Spalding<sup>11</sup> did the numerical modelling of the combustion of fuel sprays in 3-D can combustors and presented the predictions of hydrodynamic and thermodynamic properties of flow in a 3-D can combustor. The flow is three-dimensional, steady, incompressible, turbulent, and chemically reacting. The predictions were based on the numerical solution of the transport equations for the components of the mean velocity, the pressure, the kinetic energy of turbulence and its dissipation rate, the stagnation enthalpy, the concentrations of fuel droplets in five size ranges, and the concentration of gaseous fuel before and after the occurrence of a chemical reaction. In the fuel spray analysis, vaporisation-plus-combustion process around the droplet was taken into account. The numerical solution procedure provides a useful tool for investigating gas turbine combustion chamber problems.

### 3. NUMERICAL STUDY

A numerical study was performed for obtaining the flow field characteristics of annular gas turbine combustor. It involves solving the following equations:

- (a) Continuity equation
- (b) Momentum equation
- (c) Energy equation
- (d) Turbulence-modelling equations

(a) Continuity Equation

$$\frac{\partial}{\partial X_i}(\rho u_i) = 0$$

(b) Momentum Equation

$$\begin{aligned} & \frac{\partial}{\partial X_j}(\rho u_i u_j) \\ &= -\frac{\partial p}{\partial X_i} + \frac{\partial}{\partial X_j} \left[ \mu \left( \frac{\partial u_i}{\partial X_j} + \frac{\partial u_j}{\partial X_i} - \frac{2}{3} \delta_{ij} \frac{\partial u_k}{\partial X_k} \right) \right] \\ & \quad + \frac{\partial}{\partial X_j}(-\overline{\rho u_i' u_j'}) + F_i \end{aligned}$$

(c) Energy Equation

$$\begin{aligned} & \frac{\partial}{\partial X_i} [u_i(\rho E + p)] \\ &= \frac{\partial}{\partial X_i} \left( k_{eff} \frac{\partial T}{\partial X_i} - \sum_j h_j j_j + u_j (\tau_{ij})_{eff} \right) \end{aligned}$$

(d) Turbulence Modelling Equations

The turbulence modelling has been done using (RNG)  $k-\epsilon$ . The following equations are being solved:

$$\rho \frac{Dk}{Dt} = \frac{\partial}{\partial X_i} \left[ \alpha_k \mu_{eff} \frac{\partial k}{\partial X_i} \right] + G_k - \rho \epsilon - Y_M$$

where

$$Y_M = 2\rho\epsilon \left( \frac{k}{a^2} \right)$$

and

$$\rho \frac{D\epsilon}{Dt} = \frac{\partial}{\partial X_i} \left[ \alpha_\epsilon \mu_{eff} \frac{\partial \epsilon}{\partial X_i} \right] + C_{1\epsilon} \frac{\epsilon}{k} G_k - C_{2\epsilon} \rho \frac{\epsilon^2}{k} - R$$

where

$$R = \frac{C_\mu \rho \eta^3 \left( 1 - \frac{\eta}{\eta_0} \right) \epsilon^2}{1 + \beta \eta^3 k}$$

where  $\eta \equiv Sk/\epsilon$ ,  $\eta_0 = 4.38$ ,  $\beta = 0.012$ , and  $C_\mu = 0.0845$ . Here,  $S$  is the scalar measure of the deformation tensor and is given by

$$S \equiv \sqrt{2\Omega_{ij}\Omega_{ji}}$$

where  $\Omega_{ij}$  is the mean rate of rotation tensor and is defined by

$$\Omega_{ij} = \frac{1}{2} \left( \frac{\partial u_j}{\partial X_i} - \frac{\partial u_i}{\partial X_j} \right)$$

In the above equations,  $G_k$  represents the generation of turbulent kinetic energy due to the mean velocity gradients, and is evaluated as follows:

$$G_k = 2\mu_t S_{ij} S_{ji}$$

where the mean strain rate  $S_{ij}$  is given by

$$S_{ij} = \frac{1}{2} \left( \frac{\partial u_i}{\partial X_j} + \frac{\partial u_j}{\partial X_i} \right)$$

where  $C_{1\epsilon}$ ,  $C_{2\epsilon}$  are the model constants having the following default values derived analytically by the RNG theory:

$$C_{1\epsilon} = 1.42 \quad C_{2\epsilon} = 1.68$$

### 3.1 Discretisation of Governing Equations

A generalised non-orthogonal curvilinear finite volume technique is used to solve the governing equations. The governing equations of general convection-diffusion form are transformed into a body-fitted non-orthogonal coordinate system. Choice of this kind of coordinate system facilitates accurate representation of irregular geometries. The governing equations in the transformed coordinates are discretised using the finite volume technique. The pressure-velocity coupling is numerically implemented using the SIMPLE algorithm. A non-staggered grid layout is used for discretisation. The momentum interpolation scheme is used to obtain mass fluxes, pressure and

pressure correction at the control volume interfaces. In 3-D calculations, for certain configurations, periodic boundary conditions become necessary. Such cases are handled by overlapping the near-boundary control volumes in the periodic direction, which gives the required boundary conditions.

The above equations are solved using the SIMPLE algorithm, which is basically an iterative approach, where some innovative physical reasoning is used to construct the next iteration from the results of the previous iteration. The thought process<sup>13</sup> has the following steps:

- Step 1.* Start the iterative process by guessing the pressure field. Denote the guessed pressure by  $p^*$ .
- Step 2.* Use the values of  $p^*$  to solve for  $u$ ,  $v$  and  $w$  from the momentum equations. Since these velocities are those associated with the values of  $p^*$ , denote these by  $u^*$ ,  $v^*$  and  $w^*$ .
- Step 3.* Since these were obtained from guessed values of  $p^*$ , the values  $u^*$ ,  $v^*$ , and  $w^*$ , when substituted into the continuity equation, will not necessarily satisfy that equation. Hence, using the continuity equation, construct a pressure correction  $p'$  which when added to  $p^*$  brings the velocity field more into agreement with the continuity equation. That is the corrected pressure  $p$  where  $p = p^* + p'$ . Corresponding velocity corrections  $u'$ ,  $v'$ , and  $w'$  can be obtained from  $p'$  such that  $u = u^* + u'$ ,  $v = v^* + v'$  and  $w = w^* + w'$ .
- Step 4.* For turbulent flows, turbulence model equations for  $k$  and  $\epsilon$  also solved.
- Step 5.* Designate the new value  $p$  on the left hand side in *Step 3* as the new value of  $p^*$ . Return to *Step 2*, and repeat the process until a velocity field is found that satisfies the continuity equation. When this is achieved, the correct flow field will be obtained.

## 4. COMBUSTOR MODELLING

Many types of combustors, differing widely in size and method of fuel injection, have been designed. However, close inspection reveals that many aerodynamic features are common to all the systems. In the diffuser and the annulus, the main objectives are to reduce the flow velocity and to distribute the air in the prescribed quantities to all the combustor zones, while maintaining uniform flow condition with no parasitic losses or flow recirculation of any kind.

### 4.1 Mixing Process

The mixing processes are of paramount importance in the combustion and dilution zones of the combustor. In the primary zone, good mixing is essential for achieving high burning rates and to minimise soot and nitric oxide formation, whereas the attainment of a satisfactory temperature distribution (pattern factor) in the exhaust gases is very much dependent on the degree of mixing of air and the combustion products in the dilution zone. Unfortunately, thorough mixing can be achieved only at the expense of pre-diffuser length and total pressure loss. Thus, the primary objective of combustor design is to achieve satisfactory mixing within the liner and a stable flow pattern throughout the entire combustor, with no parasitic losses and minimum length of pre-diffuser and total-pressure loss.

### 4.2 Combustor Configuration

The combustor configuration has been illustrated in Fig.1. The air leaving the compressor enters the pre-diffuser section, where the large portion of the velocity head will be recovered, and then the air enters into the dump region of the diffuser. In this region, the flow is split and it enters the flame tube and the surrounding feed annuli. The dump diffuser-combustor design parameters are governed by the geometry and flow properties. These include the pre-diffuser length and area ratio, dump gap, velocity distribution, and turbulence level at the compressor exit. The other considerations are the locations of support struts and atomiser. These subcomponents should be designed and placed such that these have minimal effect on the pressure and the combustor

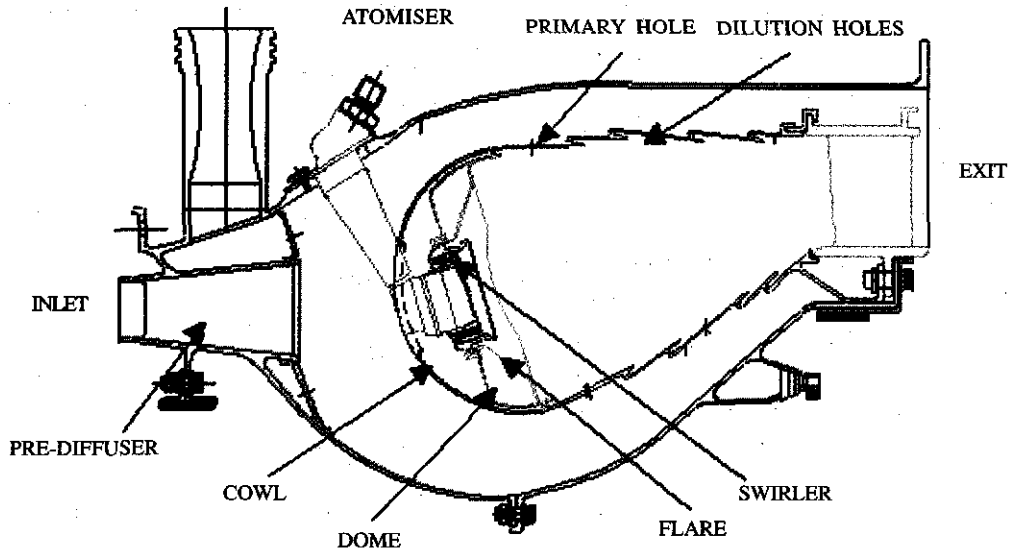


Figure 1. Combustor configuration

exit temperature quality. The diffuser system should be so designed that the total-pressure loss is minimised. Further, it should deliver the desired air flow rate into various regions of the combustor.

The flow-split among outer annuli, inner annuli, and the central streams are strong functions of the dump gap ratio, which in turn affects the overall combustor total-pressure loss. Figure 2 shows the model of the combustor incorporating various features, such as swirler with 12 blades, air-blast atomiser, cowl, dome, flare, and primary hole, secondary, and cooling ring holes. Owing to the symmetry of

the geometry, 20° sector of the 3-D combustor, as shown in Fig. 2, is used for analysis. The flat vane swirler has been modelled with a constant vane angle of 50°.

## 5. GEOMETRY GRID GENERATION

In the present study, unstructured grid has been employed due to the complexity of geometry of the combustor. The 3-D modelling of the combustor (20° sector) has been done using the pre-processors GAMBIT and CATIA. The 3-D modelling has been done incorporating various features, such as the

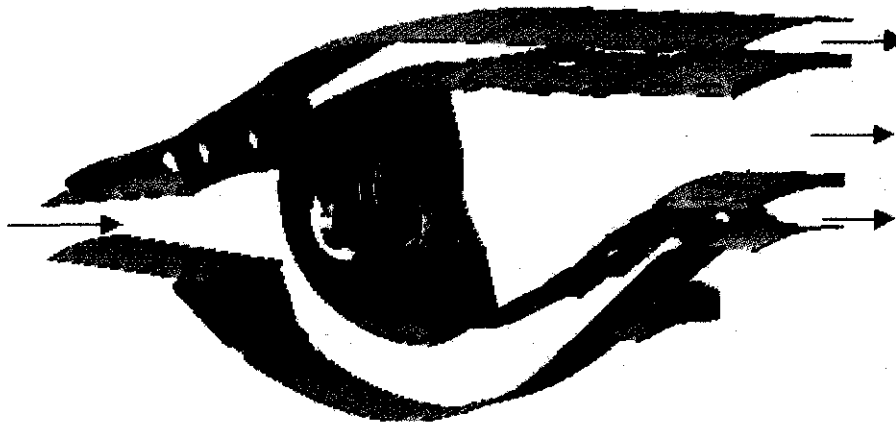


Figure 2. Three-dimensional modelling of the gas turbine combustor (20° sector)

swirler vane passages, pintle, air-blast atomiser, swirl cone, primary hole, dilution holes, and cooling ring holes. A grid size of 8.7 lakhs (tetrahedral cell) has been employed.

## 6. BOUNDARY CONDITIONS

The problem taken up in this study has three types of boundaries. These are inlet, outlet, and the wall. These boundary conditions have been prescribed in the following ways:

### 6.1 Inlet Boundary

The velocity boundary condition is used to define the flow velocity along with all relevant scalar properties of the flow at the flow inlet. The velocity magnitude and direction, the velocity components or the velocity magnitude normal to the boundary specifies flow inlet velocity. The inlet velocity used in the present study is 198.5 m/s.

### 6.2 Outlet Boundary

The outlet boundary condition is used to model the flow at exit where the details of the flow velocity and pressure are not known prior to solving the problem. As these variables were not known for the case under study, the outlet boundary condition was applied for the combustor exit. When this condition was specified, the code extrapolated the required information from the interior. In the present study, there are five outlets, the flow rate weighting has been set to indicate what fraction of total flow rate takes place through the given boundary. Table 1 gives bleed mass flow at various locations. This mass flow-split is based on the design consideration specified by the user.

### 6.3 Wall Boundary

In any flow, Reynolds number of the flow becomes very low and turbulent fluctuations are damped considerably, near the walls. The laminar viscosity starts to play a significant role. In the present case, walls were assumed to be adiabatic with no-slip condition. The standard wall functions were used to calculate the variables at the near wall-cells and the corresponding quantities on the wall.

Table 1. Mass flow split at various locations

Location	Percentage of total mass flow
Outer	6.97
Inner front (rotor)	3.94
Inner rear	4.01
Customer bleed	0.73
Flame tube	84.35

## 7. RESULTS & DISCUSSION

The flow inside the annular combustor has been analysed for a 20° sector of a 3-D model for predicting the flow field inside the combustor under isothermal flow conditions. The various blockages in the geometry like support strut at pre-diffuser, atomiser, and swirl cone, were included in the present analysis. The flow characteristics in the modelled annular gas turbine combustor were evaluated for isothermal flow condition with inlet velocity of 198.5 m/s and at 895.7 K.

The Fig. 3 shows velocity contours plot of flow field from the pre-diffuser inlet to the combustor exit. There is a clear re-circulation zone (Fig. 4) downstream of the swirler. This re-circulation zone is formed due to the effect of the radial pressure gradient created by the swirler and also due to the interaction of opposing primary jets, which have been modelled carefully. This re-circulation zone is very important for flame stabilisation in the primary zone so that the flame remains anchored to the atomiser and almost complete burning must take place in the primary zone to get a good exit pattern factor.

From Figs 5 and 6, it can be seen that the modelling of the primary hole and dilution holes results in the corresponding air jets being generated. The primary opposing jets help in re-circulating a part of the primary air to aid in combustion in the primary zone. The primary opposing jets penetrate almost radially into the combustor and rise to a toroidal central re-circulation zone in the head of the combustor. This zone is a prerequisite for the stable combustion. The function of the dilution air jet is to mix with the products of combustion to cool these to a value acceptable by the turbine and also to reduce the pattern factor at the exit of the combustor.

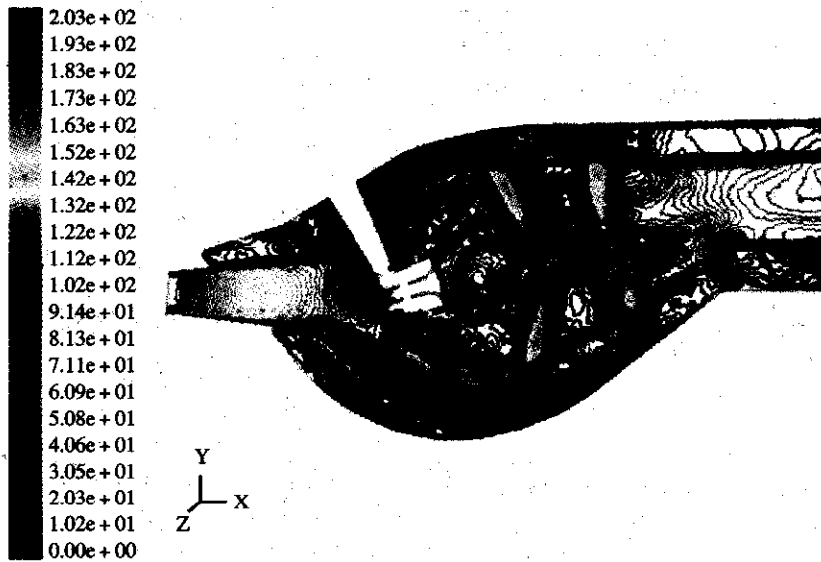


Figure 3. Velocity contours at 10° plane

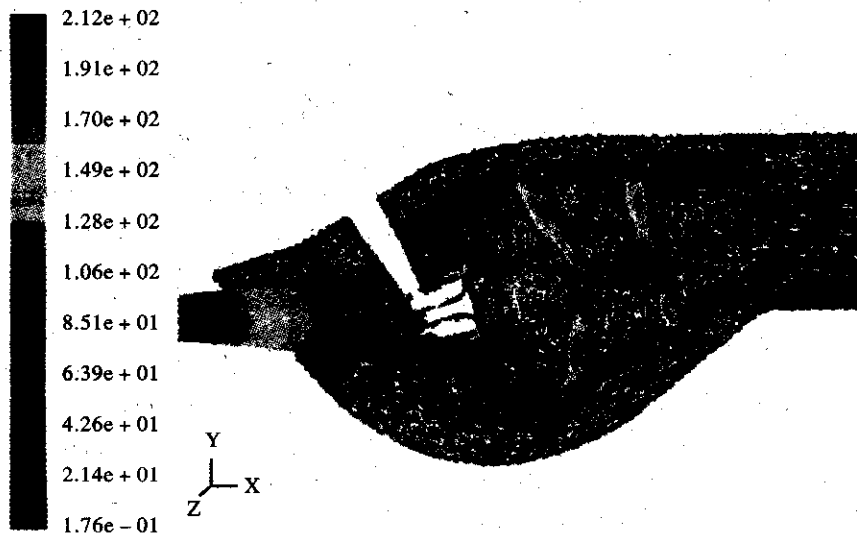


Figure 4. Velocity vectors at 10° plane

The total pressure (Fig. 7) drops across the combustor due to various blockages like the atomiser mount, the swirler, the swirl cone, and the pressure drop due to flow across the primary hole, secondary, dilution, and the cooling ring holes. Also, the pressure drops due to the skin friction along the walls of the combustor casing, the flame tube, the swirler, and the swirl cone. The total-pressure drop across the combustor for the case under consideration was 6.85 per cent.

The static pressure contours (Fig. 8) show an increase in static pressure in the dump diffuser. The static pressure recovery coefficient ( $C_{p \text{ actual}} = \Delta P_s / (0.5 \rho u^2)$ ) was 0.612 for the case under consideration. The ideal pressure recovery coefficient for the diffuser [ $C_{p \text{ ideal}} = 1 - (A_1/A_2)^2$ ] is equal to 0.63809. The pressure recovery effectiveness, which represents the ability of the diffuser to achieve ideal recovery characteristics, is the ratio of the  $C_{p \text{ actual}}$  to the  $C_{p \text{ ideal}}$ . Thus for the above case, the

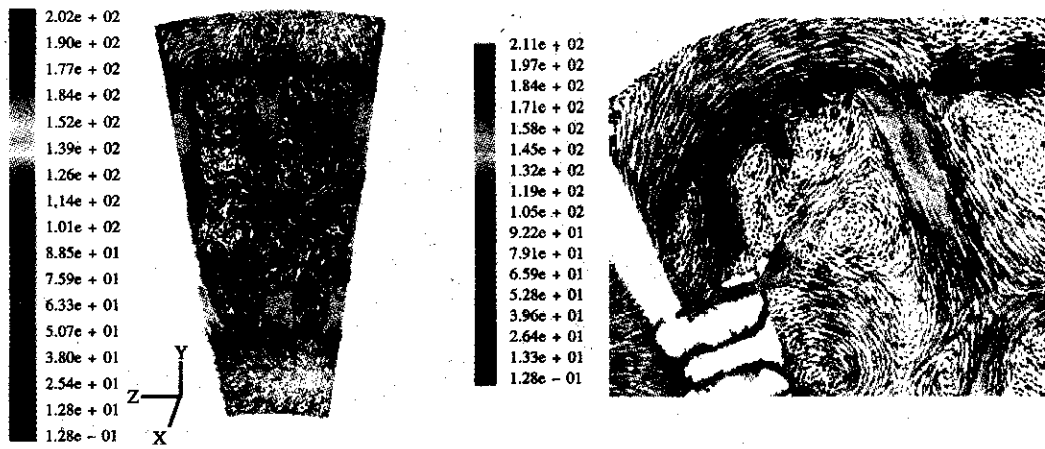


Figure 5. Flow through primary hole

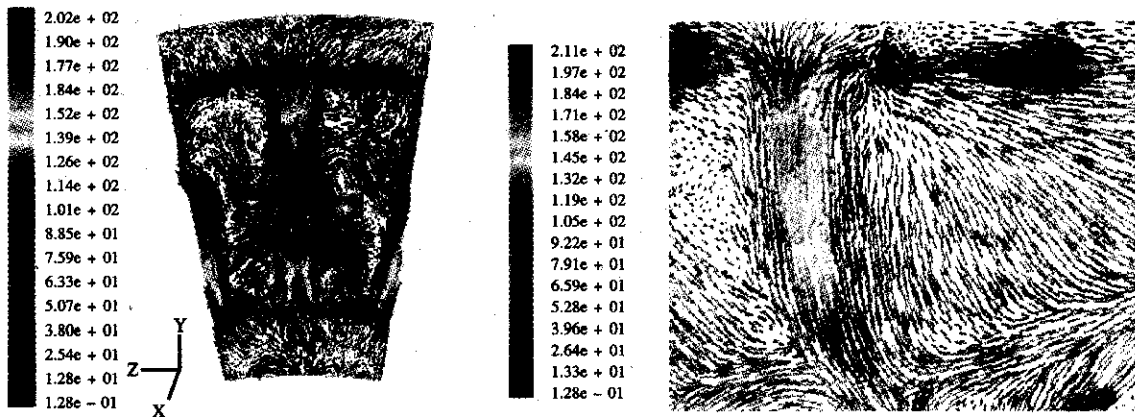


Figure 6. Flow through dilution holes

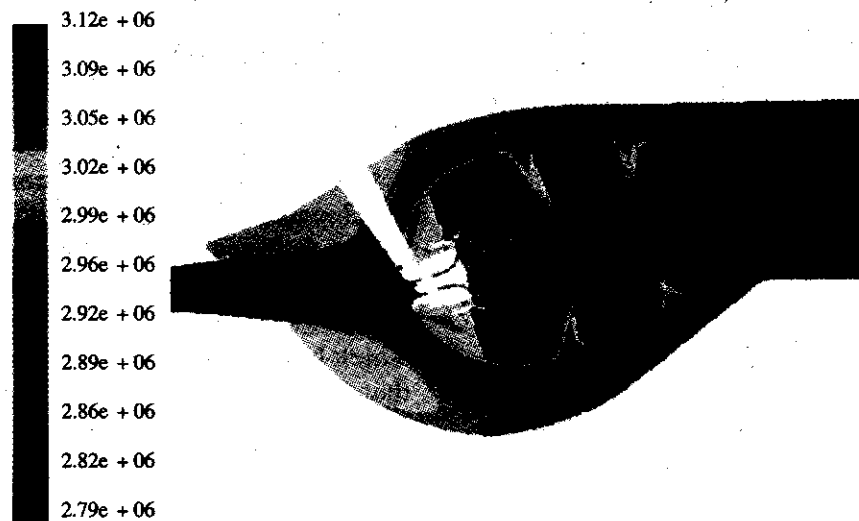


Figure 7. Total pressure contours

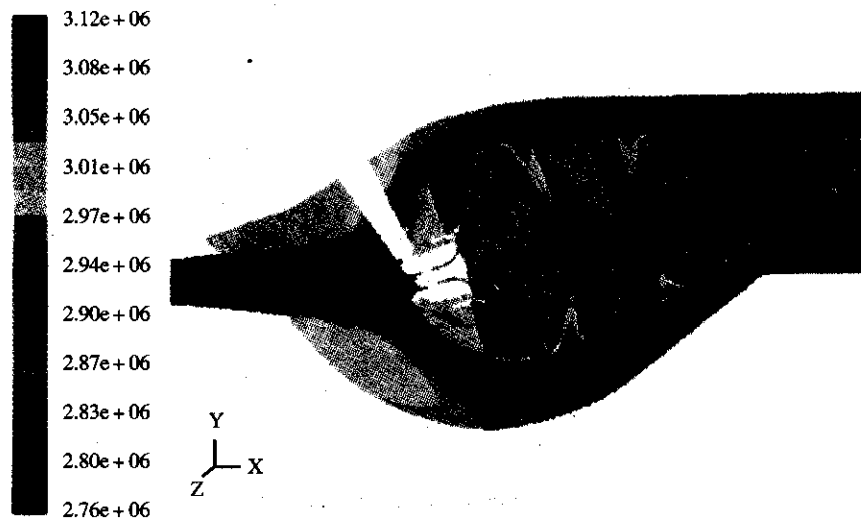


Figure 8. Static pressure contours

pressure recovery effectiveness achieved was equal to 95.9 per cent, which is a very good value and it shows that the diffuser design and performance are quite good.

### 7.1 Parametric Study for Cold Flow

The total pressure loss is influenced by the inlet velocity. The design inlet velocity of the combustor is 198.5 m/s, this is considered for the basic analysis. For the parametric study, the velocity was reduced by 10 per cent, and then by 20 per cent of the design velocity. Further, it was increased by 10 per cent, and then by 20 per cent of the design inlet velocity. Thus, the parametric study has been carried out varying the inlet velocity from 158.8 m/s to 238.2 m/s in steps of 19.85 m/s. Table 2 shows how the total-pressure loss, velocity outlet of flame tube, and the static pressure recovery coefficient vary with variation in the inlet velocity.

The total-pressure loss is caused by friction and acceleration accompanying heat addition. The total-pressure loss is mainly influenced by turbulence rather than by heat addition. In the present study, cold losses due to friction and turbulence come into play. Figure 9 shows the total-pressure loss across the combustor, which clearly shows the increase of total-pressure loss as the inlet velocity increases.

Figure 10 shows the variation of static pressure recovery coefficient with inlet velocity. As the

Table 2. Results of parametric study

Velocity inlet (m/s)	Velocity at flame tube outlet (m/s)	Total-pressure loss (%) ( $\Delta P_o/P_{03}$ )	St. Prs. Rec. Coeff. $C_p = \Delta P_o / (0.5 * \rho v^2)$
158.8	52.83	4.41	0.609
178.65	59.50	5.54	0.611
198.50	67.07	6.85	0.612
218.35	73.71	8.31	0.613
238.20	80.55	9.87	0.616

inlet velocity increases, the static pressure recovery coefficient increases marginally. Figure 11 shows the variation of flame tube outlet velocity with the inlet velocity.

## 8. VALIDATION

The validation of total-pressure loss for the present combustor configuration could not be carried out as the proposed combustor geometry is under development and no experimental data are available. However, Balasubramium<sup>12</sup> has satisfactorily validated the FLUENT code being used, earlier for the baseline combustor configuration. Some typical results<sup>13</sup>, which have been reproduced in Figs 7 and 8, show that computational fluid dynamics results are as expected.

A comparison between the experimental and the predicted results has been shown in Fig 12. From the graph it is clear that the experimental

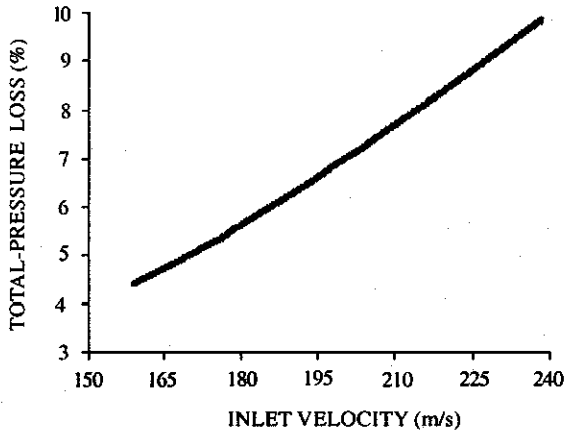


Figure 9. Variation of total-pressure loss with inlet velocity

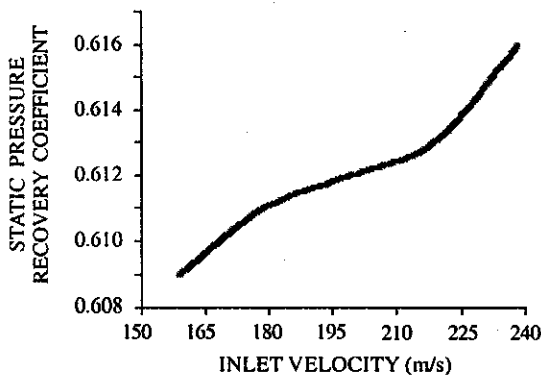


Figure 10. Variation of static pressure recovery coefficient with inlet velocity.

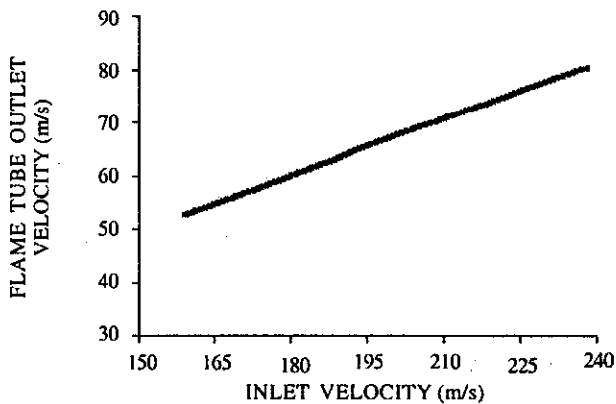


Figure 11. Variation of flame tube outlet velocity with inlet velocity.

values are higher than the predicted values. This is mainly attributed to the presence of appendages and struts, and other obstructions in the flow path in the experimental model and accuracy of the experiments. However, it may be noted that the predicted results in the present study are quite plausible, and therefore, these can be used with confidence.

### 9. CONCLUSIONS

A numerical study has been carried out to calculate the non-reacting flows typical of aero gas turbine combustor geometry, which contain a combination of swirling and re-circulating flows. Some of the important conclusions are:

- A strong re-circulation zone is created due to the effect of radial pressure gradient, which results from the effect of swirler and due to the interaction of opposing primary and dilution jets.

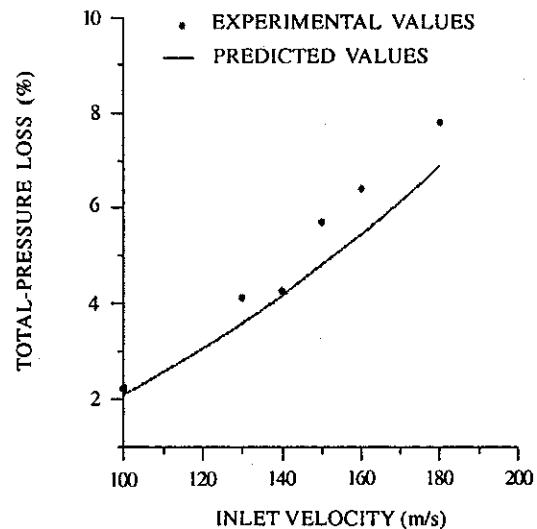


Figure 12. Total-pressure loss validation

- The static pressure recovery coefficient and diffuser effectiveness show that the diffuser design is quite good for wide range of inlet velocity. Increasing the inlet velocity causes marginal improvement in static pressure recovery.
- With an increase in the inlet velocity, the total-pressure loss also increases.

## REFERENCES

1. Crocker, D.S.; Nickolaus, D. & Smith, C.E. CFD modelling of a gas turbine combustor from compressor exit to turbine inlet. *ASME J. Engg. Gas Turbine Power*, 1999, **121**, 89-95.
2. Sokolov, K.Y.; Tumanovsky, A.G. & Gutnik, M.N. Mathematical modelling of an annular gas turbine combustor. *ASME J. Engg. Gas Turbine Power*, 1995, **117(1)**, 94-98.
3. Su, K. & Zhou, C.Q. Numerical modelling of gas turbine combustor integrated with diffuser. *In Proceedings of the 34<sup>th</sup> National Heat transfer Conference*, Pittsburg, Pennsylvania.
4. Relation, J.L. & Battaglioli, W.F. Ng. Numerical simulations of non-reacting flows for industrial gas turbine combustor geometry. *ASME J. Engg. Gas Turbine Power*, 1998, **120**, 460-67.
5. Karki, K.C.; Oechsle, V.L. & Mongia, H.C. A computational procedure for diffuser-combustor flow interaction analysis. *ASME J. Engg. Gas Turbine Power*, 1992, **114(1)**, 1-7.
6. Agarwal, J.S.; Kapat, T.T. & Yang. An experimental/computational study of air flow in the combustor system of a gas turbine for power generator. *ASME J. Engg. Gas Turbine Power*, 1998, **120**, 24-33.
7. Arthur, H. Lefebvre. Gas turbine combustion. Hemisphere Publishers Corp, 1993.
8. Versteeg, H.K. & Malalasekera, W. An introduction to computational fluid dynamics: The finite volume method. Longman Group Ltd, 1995.
9. Cohen, G.F.C.; Rogers & Saravanamuttoo, H.I.H. Gas turbine theory. Longman Group Ltd, 1998.
10. Ganesan, V. Gas turbines. Tata McGraw-Hill Publishing Co Ltd, 1999.
11. Ganesan, V. & Spalding, D.B. Numerical modelling of combustion of fuel sprays in 3-D can combustors. *In Proceedings of the 4<sup>th</sup> Symposium (International) on Air-breathing Engines*. USA, 1979. pp. 177-86.
12. Balasubranium, V. Numerical prediction of flow and combustion in a gas turbine combustion system. I.C Engines Lab, I.I.T Madras, Chennai, 2001. M.S Thesis.
13. Anderson, John D. (Jr.) Computational fluid dynamics. McGraw-Hill Inc, 1995.